Dynamic fracture with a continuum-kinematics-based peridynamic and a phase-field approach

Kai Friebertshäuser[1,*], **Marita Thomas**[2,3], **Sven Tornquist**[2,3], **Kerstin Weinberg**[1], and **Christian Wieners**[4]

[1] Chair of Solid Mechanics, University of Siegen, Siegen, Germany

[2] Weierstrass Institute for Applied Analysis and Stochastics, Berlin, Germany

[3] FU Berlin, Germany

[4] Institute of Applied and Numerical Mathematics, KIT, Karlsruhe, Germany

The notion of dynamic fracture with continuum-kinematics-based peridynamics is presented in this work. A geometrically precise version of peridynamics called continuum-kinematics-based peridynamics adds surface- or volume-based interactions to the traditional peridynamic bonds, accurately capturing the finite deformation kinematics. The point families produced from the horizon of the material points are used to construct the surfaces and volumes taken into account for these non-local interactions.

In continuum kinematics-based peridynamics, the traditional bond-stretch damage technique is insufficient for fracture. Due to the loss of strength in the internal force densities of the material points, it is now extended to the surface- and volume-based interactions by new failure factors. Numerical examples demonstrate that the proposed approach effectively manages crack propagation, impact damage, and spontaneous crack initiation under dynamic loading circumstances with large deformations. When the results are compared to phase-field calculations, there is a remarkable agreement concerning the damage patterns.

1 Introduction

In computational mechanics, predicting fracture propagation and material degradation is still very difficult. Numerous computational techniques, including damage models or discontinuous finite element discretizations [1–3], and phase-field fracture simulations [4–6], have been used to solve fracture problems. The classical continuum mechanics assumption of a homogeneous bulk material forms the basis for each method. Because peridynamics represents the material in a non-local form, it enables an alternative approach to fracture. Peridynamics, which Silling first developed [7, 8], uses integral equations to explain the relative forces and displacements between material points. There are no concepts like stress or strain, and a material point's behavior is only characterized by how it interacts with other material points.

In order to account for a material's Poisson ratio different than $1/4$ for 3D issues, the initial peridynamic notions were limited to the interaction of bonds. This issue is addressed by other formulations, such as ordinary state-based peridynamics and non-ordinary state-based peridynamics. Javili, McBride, and Steinmann recently proposed a novel method for reformulating peridynamics [9–11]. This geometrically precise formulation uses an analogy to classical continuum mechanics, and it is built from the ground up to correctly describe the material's lateral contraction. Bond-, surface- and volume-based interactions – which correspond to the invariants of a general deformation – are introduced as three different forms of material point interactions. Recently, correlations between the material parameters of continuum-kinematics-based peridynamics and isotropic linear elasticity were developed for two- and three-dimensional problems [12, 13].

The new continuum-based peridynamics kinematics necessitate a new understanding of damage and fracture. It is no longer sufficient to think of material damage as a bond-based event because of the three different kinds of interactions. Thus, we extend the force density of the material, which is also extended by a density linked to contact, by kinematic variables that account for the loss of load-carrying capability. In this method, impact damage, as well as crack nucleation and propagation, may be represented. To the authors' knowledge, this is the first concept of damage in the continuum-kinematics-based peridynamics paradigm.

The structure of this document is as follows. First, the terminology and necessary theory of continuum-kinematics-based peridynamics are introduced in Section 2. The core of the paper is Section 3, where we provide our damage model. Next, there are numerical examples in Sections 4-6. Section 4 begins with a model validation using a straightforward 2D crack growth for a mode I tension test. Following that, Section 5 presents the crack initiation caused by reflected impact waves using the example of a curved bar, which are quantitatively compared to phase-field calculations [14].

* Corresponding author: e-mail kai.friebertshaeuser@uni-siegen.de, phone +49 0271 740 2185

2 Theory of continuum-kinematics-based peridynamics

In peridynamics, a body is represented by a set of N points in Euclidean space $\mathbb{R}^3$, and the dynamics is depicted by the movement of these points. The point position in material configuration is described by $\boldsymbol{X}^i$ and in current configuration as

$$\boldsymbol{x}^i = \boldsymbol{X}^i + \boldsymbol{u}(\boldsymbol{X}^i, t) \, ,$$

with the displacement vector $\boldsymbol{u}(\boldsymbol{X}^i, t)$ and $i = 1, \ldots, N$. Points interact only with other points inside of their specified *neighborhood* $\mathcal{H}_1^i$, which is defined as the set of points inside the spherical space with the radius $\delta \in \mathbb{R}^+$, also called the *horizon* δ. Accordingly,

$$\mathcal{H}_1^i = \left\{ \boldsymbol{X}^j \in \mathcal{B}_0 \mid 0 < \left| \boldsymbol{X}^j - \boldsymbol{X}^i \right| \leq \delta \right\} \quad \forall \, \boldsymbol{X}^i \in \mathcal{B}_0$$

includes all points $\boldsymbol{X}^j$ inside the horizon of point $\boldsymbol{X}^i$ in the reference configuration of the body $\mathcal{B}_0$.

The equation of motion for point i reads

$$\rho \, \ddot{\boldsymbol{u}}(\boldsymbol{X}^i, t) = \boldsymbol{b}_0^{\mathrm{int}}(\boldsymbol{X}^i, t) + \boldsymbol{b}_0^{\mathrm{ext}}(\boldsymbol{X}^i, t) \qquad \forall \, \boldsymbol{X}^i \in \mathcal{B}_0, \; t \geq 0 \tag{1}$$

with the density ρ, the point acceleration vector $\ddot{\boldsymbol{u}}$, and the point force density vectors $\boldsymbol{b}_0^{\mathrm{int}}$ and $\boldsymbol{b}_0^{\mathrm{ext}}$, which denote force per unit undeformed volume. The external force density $\boldsymbol{b}_0^{\mathrm{ext}}$ results from the external forces that are acting on the body and the internal force density $\boldsymbol{b}_0^{\mathrm{int}}$ from the interactions between the individual material points. Because all equations are mapped to the reference configuration, peridynamics can be thought of as a Lagrangian particle approach. In the following, the notation $\boldsymbol{u}^i = \boldsymbol{u}(\boldsymbol{X}^i, t)$ and $\boldsymbol{b}_0^{\mathrm{int},\,i} = \boldsymbol{b}_0^{\mathrm{int}}(\boldsymbol{X}^i, t)$ will be used for improved readability. We employ the Velocity-Verlet explicit time integration approach [15] because all of our simulations take place over small time spans.

For calculating the internal force density, numerous peridynamics formulations are available, and each one is based on the non-local interactions between the material points. The utilization of three separate interactions, also known as one-, two-, and three-neighbor interactions, makes continuum-kinematics-based peridynamics special (see Fig. 1). Correspondingly, for continuum-kinematics-based peridynamics, $\boldsymbol{b}_0^{\mathrm{int},\,i}$ is the sum of the internal force densities of these interactions, thus

$$\boldsymbol{b}_0^{\mathrm{int},\,i} = \boldsymbol{b}_1^{\mathrm{int},\,i} + \boldsymbol{b}_2^{\mathrm{int},\,i} + \boldsymbol{b}_3^{\mathrm{int},\,i} \, .$$

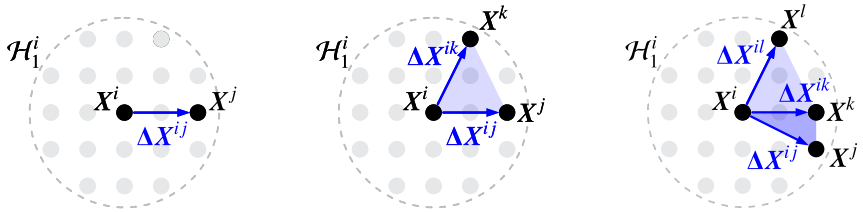

Fig. 1: Illustration of one-, two-, and three-neighbor interactions of point $\boldsymbol{X}^i$

The *one-neighbor interaction* of point i and j, in standard peridynamics also called the *bond*, is defined in material and current configuration as

$$\boldsymbol{\Delta X}^{ij} = \boldsymbol{X}^j - \boldsymbol{X}^i \, , \qquad \boldsymbol{\Delta x}^{ij} = \boldsymbol{x}^j - \boldsymbol{x}^i \, .$$

One-neighbor interactions can be interpreted as line elements with the initial length L^{ij} in material notation and the deformed length l^{ij} in current configuration. These so called relative length measures of the one-neighbor interaction are defined as

$$L^{ij} = \left| \boldsymbol{\Delta X}^{ij} \right| \, , \qquad l^{ij} = \left| \boldsymbol{\Delta x}^{ij} \right| \, .$$

It is assumed, that all one-neighbor interactions of point i contribute equally. Therefore, an effective one-neighbor volume is defined as

$$V_1^i = \frac{V_{\mathcal{H}}^i}{N_1^i} \, ,$$

with N_1^i being the number of one-neighbor interactions for point i and the neighborhood volume

$$V_{\mathcal{H}}^i = \begin{cases} \beta^i \, \frac{4}{3} \, \pi \, \delta^3 & \text{(3D problems)} \\ \beta^i \, \pi \, \delta^2 & \text{(2D problems)} \end{cases}$$

with the factor $\beta^i \in [0,1]$ that takes the fullness of the neighborhood into account. As an example, it applies $\beta^i = 1$ if the neighborhood of point i is completely inside the body $\mathcal{B}_0$. On the other hand, if the neighborhood of point i is partially outside the body $\mathcal{B}_0$, the factor $\beta^i < 1$ works as a correction factor to the volume $V_{\mathcal{H}}^i$.

The force density due to one-neighbor interactions is defined as

$$\boldsymbol{b}_1^{\mathrm{int},\,i} = \int_{\mathcal{H}_1^i} C_1 \left(\frac{1}{L^{ij}} - \frac{1}{l^{ij}} \right) \boldsymbol{\Delta x}^{ij} \, \mathrm{d}V_1^i \,, \tag{2}$$

with the one-neighbor interaction constant C_1. The constant C_1 can be interpreted as a resistance against the length change of one-neighbor interactions and is defined as $C_1 = \frac{24\mu}{\pi\delta^3}$ for 2D problems [12] and as $C_1 = \frac{30\,\mu}{\pi\,\delta^4}$ for 3D problems [13] depending on the first and second Lamé parameters $\lambda = \frac{E\,\nu}{(1+\nu)(1-2\nu)}$ and $\mu = \frac{E}{2(1+\nu)}$.

Two-neighbor interactions are area elements, respectively triangles, spanned by the points $\boldsymbol{X}^i$, $\boldsymbol{X}^j$ and $\boldsymbol{X}^k$. They are constructed by two corresponding one-neighbor interactions $\boldsymbol{\Delta X}^{ij}$ and $\boldsymbol{\Delta X}^{ik}$ of point i. One important condition is that the distance between the points $\boldsymbol{X}^j$ and $\boldsymbol{X}^k$ needs to be bounded by the horizon δ. Therefore, the set of all corresponding point-sets for two-neighbor interactions of point i is defined as

$$\mathcal{H}_2^i = \left\{ \left(\boldsymbol{X}^j, \boldsymbol{X}^k\right) \in \mathcal{H}_1^i \times \mathcal{H}_1^i \mid 0 < \left| \boldsymbol{X}^j - \boldsymbol{X}^k \right| \leq \delta \right\} \quad \forall\, \boldsymbol{X}^i \in \mathcal{B}_0 \,.$$

The deformation of two-neighbor interactions is mainly described by the relative area measure, in material and current notation defined as

$$\boldsymbol{A}^{ijk} = \boldsymbol{\Delta X}^{ij} \times \boldsymbol{\Delta X}^{ik} \,, \qquad \boldsymbol{a}^{ijk} = \boldsymbol{\Delta x}^{ij} \times \boldsymbol{\Delta x}^{ik} \,,$$

and as scalar quantities the areas

$$A^{ijk} = \left| \boldsymbol{A}^{ijk} \right| \,, \qquad a^{ijk} = \left| \boldsymbol{a}^{ijk} \right| \,.$$

The force density due to two-neighbor interactions is defined as

$$\boldsymbol{b}_2^{\mathrm{int},\,i} = \int_{\mathcal{H}_2^i} 2\,C_2\,\boldsymbol{\Delta x}^{ik} \times \left(\frac{1}{A^{ijk}} - \frac{1}{a^{ijk}} \right) \boldsymbol{a}^{ijk} \, \mathrm{d}V_2^i \,, \tag{3}$$

with the effective two-neighbor volume

$$V_2^i = \frac{\left(V_{\mathcal{H}}^i\right)^2}{N_2^i} \,.$$

The number of two-neighbor interactions of point i is N_2^i. The two-neighbor interaction constant C_2 can be interpreted as a resistance against the area change and is defined as $C_2 = \frac{27}{8\pi\delta^6}(\lambda - \mu)$ for 2D problems [12] and as $C_2 = 0$ for 3D problems [13].

Three-neighbor interactions are volume elements, precisely tetrahedrons, spanned by the points $\boldsymbol{X}^i$, $\boldsymbol{X}^j$, $\boldsymbol{X}^k$ and $\boldsymbol{X}^l$. They are constructed by the three corresponding one-neighbor interactions $\boldsymbol{\Delta X}^{ij}$, $\boldsymbol{\Delta X}^{ik}$ and $\boldsymbol{\Delta X}^{il}$ of point i. For a valid three-neighbor interaction, the conditions

$$0 < \left| \boldsymbol{X}^j - \boldsymbol{X}^k \right| \leq \delta \,, \qquad 0 < \left| \boldsymbol{X}^j - \boldsymbol{X}^l \right| \leq \delta \,, \qquad 0 < \left| \boldsymbol{X}^k - \boldsymbol{X}^l \right| \leq \delta \,,$$

must be met. Consequently, the set of all corresponding point-sets for three-neighbor interactions of point i is defined as

$$\begin{aligned} \mathcal{H}_3^i = \Big\{ \left(\boldsymbol{X}^j, \boldsymbol{X}^k, \boldsymbol{X}^l\right) \in \mathcal{H}_1^i \times \mathcal{H}_1^i \times \mathcal{H}_1^i \mid\; & 0 < \left| \boldsymbol{X}^j - \boldsymbol{X}^k \right| \leq \delta \,, \\ & 0 < \left| \boldsymbol{X}^j - \boldsymbol{X}^l \right| \leq \delta \,, \\ & 0 < \left| \boldsymbol{X}^k - \boldsymbol{X}^l \right| \leq \delta \Big\} \quad \forall\, \boldsymbol{X}^i \in \mathcal{B}_0 \,. \end{aligned}$$

The deformation of three-neighbor interactions is mainly described by the relative volume measure, in material and current notation defined as

$$V^{ijkl} = \boldsymbol{A}^{ijk} \cdot \boldsymbol{\Delta X}^{il} \,, \quad v^{ijkl} = \boldsymbol{a}^{ijk} \cdot \boldsymbol{\Delta x}^{il} \,.$$

The force density due to three-neighbor interactions is defined as

$$\boldsymbol{b}_3^{\mathrm{int},\,i} = \int_{\mathcal{H}_3^i} 3\,C_3\,\left(\boldsymbol{\Delta x}^{ik} \times \boldsymbol{\Delta x}^{il}\right)\left(\frac{1}{|V^{ijkl}|} - \frac{1}{|v^{ijkl}|}\right) v^{ijkl}\,\mathrm{d}V_3^i\,, \tag{4}$$

with the effective three-neighbor volume

$$V_3^i = \frac{\left(V_{\mathcal{H}}^i\right)^3}{N_3^i}\,.$$

The number of three-neighbor interactions of point i is N_3^i. The three-neighbor interaction constant C_3 can be interpreted as a resistance against the volume change and is defined as $C_3 = \frac{32}{\pi^4\,\delta^{12}}(\lambda - \mu)$ [13].

3 Modeling damage with continuum-kinematics-based peridynamics

Damage is modeled in classical peridynamics by the failure of one-neighbor interactions. The one-neighbor interaction stretch

$$\varepsilon^{ij} = \frac{\left|\boldsymbol{\Delta x}^{ij} - \boldsymbol{\Delta X}^{ij}\right|}{\left|\boldsymbol{\Delta X}^{ij}\right|}\,,$$

and the critical one-neighbor interaction stretch $\varepsilon_c > 0$ together make up the failure quantity for the strain-based damage model, which is written as

$$d_1^{ij} = \begin{cases} 0 & \text{if } \varepsilon^{ij} > \varepsilon_c\,, \\ 1 & \text{else.} \end{cases}$$

The pointwise damage quantity D^i incorporates the whole neighborhood, and is defined as

$$D^i = 1 - \frac{\int_{\mathcal{H}_1^i} d_1^{ij}\,\mathrm{d}V_1^i}{\int_{\mathcal{H}_1^i}\mathrm{d}V_1^i}\,.$$

Since these equations do not account for interactions between two or three neighbors, they cannot be directly employed to simulate damage in the continuum-kinematics-based framework. Due to the persistence of two- or three-neighbor interactions, which still induce forces between failed points, using this damage model alone will result in scattered failure zones rather than crack paths.

The failure quantities, d_2^{ijk} and d_3^{ijkl}, for two- and three-neighbor interactions are introduced to address this issue. Here, we propose that if one or more related one-neighbor interactions fail, the related two- and three-neighbor interactions will also fail. Therefore, the failure quantities for two- and three-neighbor interactions can be defined as

$$d_2^{ijk} = \begin{cases} 0 & \text{if } d_1^{ij} = 0 \text{ or } d_1^{ik} = 0\,, \\ 1 & \text{else}\,, \end{cases} \qquad d_3^{ijkl} = \begin{cases} 0 & \text{if } d_1^{ij} = 0 \text{ or } d_1^{ik} = 0 \text{ or } d_1^{il} = 0\,, \\ 1 & \text{else}\,. \end{cases}$$

With these failure quantities, we re-define the internal force density equations (2), (3) and (4) as

$$\begin{aligned}
\boldsymbol{b}_1^{\mathrm{int},\,i} &= \int_{\mathcal{H}_1^i} d_1^{ij}\,C_1\left(\frac{1}{L^{ij}} - \frac{1}{l^{ij}}\right)\boldsymbol{\Delta x}^{ij}\,\mathrm{d}V_1^i\,, \\
\boldsymbol{b}_2^{\mathrm{int},\,i} &= \int_{\mathcal{H}_2^i} d_2^{ijk}\,2\,C_2\,\boldsymbol{\Delta x}^{ik} \times \left(\frac{1}{A^{ijk}} - \frac{1}{a^{ijk}}\right)\boldsymbol{a}^{ijk}\,\mathrm{d}V_2^i\,, \\
\boldsymbol{b}_3^{\mathrm{int},\,i} &= \int_{\mathcal{H}_3^i} d_3^{ijkl}\,3\,C_3\,\left(\boldsymbol{\Delta x}^{ik} \times \boldsymbol{\Delta x}^{il}\right)\left(\frac{1}{|V^{ijkl}|} - \frac{1}{|v^{ijkl}|}\right) v^{ijkl}\,\mathrm{d}V_3^i\,.
\end{aligned}$$

In this way, the damaging effect of the failed point interactions is considered, and they do not contribute to the internal material response.

4 Numerical results for the mode I tension test

The ability of continuum-kinematics-based peridynamics to predict crack growth for two- and three-dimensional issues is demonstrated in the following section. Therefore, a square with an edge length of l and a predefined crack of length $a = \frac{1}{2}l$ is put under tension by the model's upper and lower regions expanding at a constant speed of $v_0 = 0.005\,\mathrm{m\,s^{-1}}$.

For the 2D setup, a uniformly distributed point cloud with 200×200 points (point spacing $\Delta x = 5\,\mathrm{mm}$ and horizon $\delta = 15.075\,\mathrm{mm}$), and for the 3D setup $60 \times 60 \times 3$ points (point spacing $\Delta x = 16.7\,\mathrm{mm}$ and horizon $\delta = 50.25\,\mathrm{mm}$) are used. Both setups use the material parameters of steel, with density $\rho = 7580\,\mathrm{kg\,m^{-2}}$, Young's modulus $E = 210\,000\,\mathrm{MPa}$, and Poisson's ratio $\nu = 0.3$. The critical stretch for the 2D setup is defined as $\varepsilon_c = 4.04 \times 10^{-4}$ and for the 3D setup $\varepsilon_c = 1.78 \times 10^{-4}$.

Figure 2 displays the damage D^i for both the 2D and 3D setup. The fracture propagates and expands as anticipated for both configurations until it splits the square in half. Without the additional failure quantities d_2^{ijk} and d_3^{ijkl}, the simulations would have produced a diffuse damage field and no identifiable fracture path. As a result, our proposed damage model can be used to describe crack growth utilizing continuum-kinematics-based peridynamics.

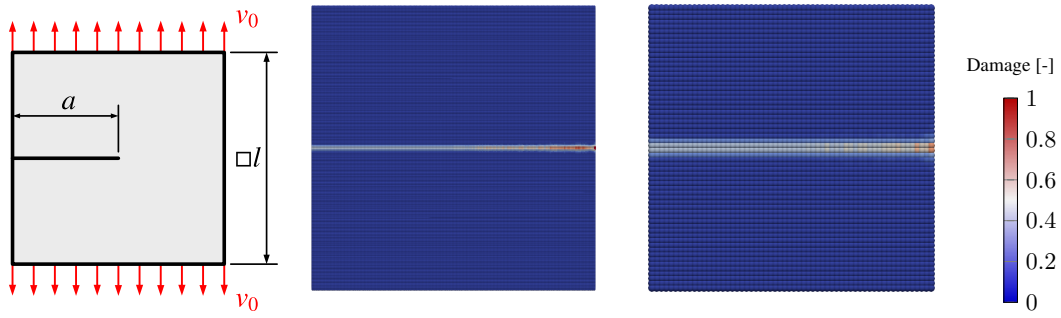

Fig. 2: Damage D^i for the 2D (left) and 3D setup (right)

5 Curved bar under pressure

In the following section, crack initiation due to impact is investigated for a two- and three-dimensional discretizations. For this purpose, a model of a curved bar is subjected to pressure waves, which are supposed to superimpose inside the material and eventually lead to crack initiation. Both setups use the material parameters of steel, as before in Section 4. The material points are spatially distributed along the curve $f(x) = \cos\left(\frac{\pi}{2}\,x\right)$ (see [14, 16] for more details on the discretizations and the material properties).

On each side of the curved bar, a pressure impulse

$$p(t) = \begin{cases} -4 \cdot \frac{p_0}{{t_1}^2} \cdot \left(t - \frac{t_1}{2}\right)^2 + p_0 & t \le t_1 \\ 0 & t > t_1 \end{cases}$$

with the pressure peak p_0 and the impulse duration t_1 is applied for one layer of material points in the left and right boundary. The pressure is applied via the external body force density $\boldsymbol{b}_0^{\mathrm{ext},\,i} = p(t)/\Delta x\,\boldsymbol{n}_{l/r}$ with the normal vector $\boldsymbol{n}_{l/r}$ for the left and right side of the bar. For the two-dimensional setup, a pressure impulse with the peak $p_0 = 4 \times 10^5\,\mathrm{N\,m^{-1}}$ and for the three-dimensional setup, $p_0 = 1 \times 10^6\,\mathrm{N\,m^{-2}}$ is used. For both setup's, the pulse has the duration $t_1 = 300\,\mu\mathrm{s}$. Remark that for 2D, the body force density $\boldsymbol{b}_0^{\mathrm{ext}}$ has the unit $[\mathrm{N\,m^{-2}}]$.

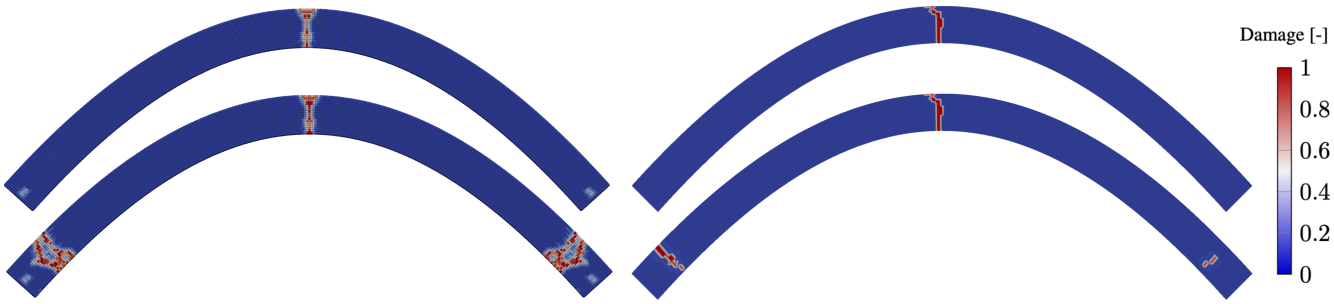

Fig. 3: Damage results of the 2D curved bar of the peridynamics (left) and phase-field simulation (right)

In Fig. 3, the damage D^i of the two-dimensional setup is shown and compared with results obtained with a corresponding phase-field calculation (see [14]). The pressure waves travel through the bar until they get reflected at the free ends, turning them into tensile waves. The peak of these tensile waves then triggers the development of a crack in the middle of the bar See also [17] for a more detailed description of the wave propagation inside of the model. Again further cracks develop when the waves continue to propagate and reflect in the model, and a further peak in tension emerges. The two-dimensional model

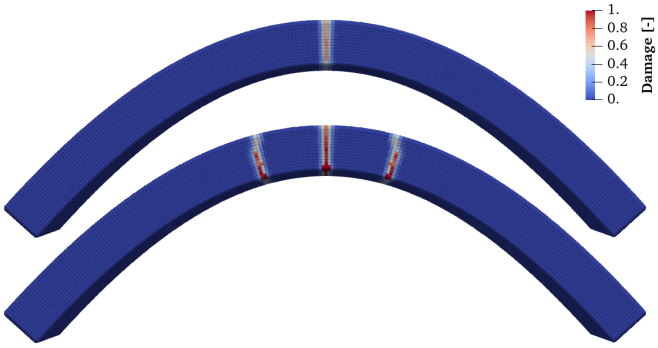

Fig. 4: Damage D^i (top) of the 3D curved bar after $t = 0.5\,\mathrm{ms}$ (top) and $t_1 = 1.4\,\mathrm{ms}$

accurately captures this pattern since these secondary cracks appear over time. It is fascinating that this effect occurs very similarly for the peridynamics and the phase-field approach, despite being fundamentally different methods.

The same behavior can also be observed with the 3D model (see Fig. 4). One crack starts in the model's center after the pressure wave's initial reflection and conversion to tensile waves. Additionally, cracking brought on by additional wave superposition can be seen. The location differs from the 2D model, although this could be explained by the several peridynamics-based continuum kinematics influencing aspects, including material characteristics and various discretizations. Further research is required in this case. Because of the much greater computational cost, we could not perform 3D calculations using the phase-field method with the same bar model.

In conclusion, it can be said that CPD can be utilized to map cracking caused by the material's reaction to wave propagation and compares well to similar results of phase-field computations.

6 Summary

In the context of CPD, this work introduces a novel approach to dynamic fracture and damage. The traditional uni-axial damage model is expanded with the addition of failure quantities for two- and three-neighbor interactions. Cracks and damage can now be described within the continuum-based framework thanks to these quantities, which deactivate two- and three-neighbor interactions if the related one-neighbor interactions fail.

Crack growth and crack initiation were two different effects that have been numerically addressed. First, we discovered that our method effectively manages the crack propagation of a mode I tension test in two- and three-dimensional simulations. Second, pressure waves are applied to a curved bar to study crack initiation. The model begins to crack due to the pressure waves superimposing and creating tensile waves. We noticed a primary crack in the model's center and secondary cracks brought on by the waves continued superposition. These effects perfectly agree with the results obtained using our phase-field approach.

Acknowledgements This work is financially supported by the German Research Foundation (DFG) in the priority programme "Variational Methods for Predicting Complex Phenomena in Engineering Structures and Materials" (SPP2256) within the project "Nonlinear Fracture Dynamics: Modeling, Analysis, Approximation, and Applications" (TH 1935/5-1, WE 2525/15-1 and WI 1430/9-1).

References

[1] X. P. Xu and A. Needleman, J. Mech. Phys. Solids **42**, 1397–1434 (1994).
[2] M. Ortiz and A. Pandolfi, International Journal for Numerical Methods in Engineering **44**, 1267–1282 (1999).
[3] T. Dally, C. Bilgen, M. Werner, and K. Weinberg, Modeling and Simulation in Engineering-Selected Problems pp. 101–126 (2020).
[4] C. Miehe and S. Mauthe, Computer Methods in Applied Mechanics and Engineering **304**, 619–655 (2016).
[5] Z. A. Wilson and C. Landis, Journal of The Mechanics and Physics of Solids **96**, 264–290 (2016).
[6] C. Bilgen and K. Weinberg, International Journal of Fracture **232**(2), 135–151 (2021).
[7] S. A. Silling, Journal of the Mechanics and Physics of Solids **48**(1), 175 – 209 (2000).
[8] S. A. Silling and E. Askari, Computers and Structures p. 10 (2005).
[9] A. Javili, A. McBride, and P. Steinmann, Journal of the Mechanics and Physics of Solids **131**(07) (2019).
[10] A. Javili, S. Firooz, A. McBride, and P. Steinmann, Computational Mechanics **66**(10) (2020).
[11] A. Javili, A. Mcbride, and P. Steinmann, Theoretical and Applied Fracture Mechanics **111**(02), 102850 (2021).
[12] E. Ekiz, P. Steinmann, and A. Javili, International Journal of Solids and Structures **238**(12), 111366 (2021).
[13] E. Ekiz, P. Steinmann, and A. Javili, Mechanics of Materials **173**(08), 104417 (2022).
[14] K. Weinberg and C. Wieners, Computer Methods in Applied Mechanics and Engineering **389**, 114330 (2022).
[15] D. J. Littlewood, Sandia National Laboratories (2015).
[16] K. Friebertshäuser, C. Wieners, and K. Weinberg, AIMS Material Science (to appear) (2022).
[17] S. Tornquist, K. Friebertshäuser, C. Wieners, K. Weinberg, and M. Thomas, submitted to PAMM (2022).